

## Article

# Research on Laboratory Testing Method of Fatigue Performance of Semi-Rigid Base Considering Spatial Stress State

Longfei Wang<sup>1</sup>, Zhizhong Zhao<sup>1</sup>, Hao Liang<sup>2</sup>, Yilong He<sup>3</sup>, Xianzhang Kang<sup>1</sup> and Meng Xu<sup>1,\*</sup> <sup>1</sup> School of Transportation and Civil Engineering, Shandong Jiaotong University, Jinan 250357, China<sup>2</sup> Shandong Luzhong Highway Construction Co., Ltd., Zibo 255030, China<sup>3</sup> Shandong Expressway Environmental Protection Building Materials Co., Ltd., Jinan 250098, China

\* Correspondence: xumeng@sdjtu.edu.cn

**Abstract:** In order to accurately assess the fatigue performance of semi-rigid base layers, this paper proposes a novel fatigue testing method for semi-rigid base layers that takes into account the spatial stress state. Based on this method, the fatigue performance of three types of reinforced semi-rigid base-layer materials (steel wire mesh, plastic geogrid, and fiberglass) was tested and compared with unreinforced materials. The fatigue strain evolution patterns of these materials were analyzed, and a fatigue strain characteristic value at the limit state was proposed as an evaluation index for the fatigue failure of base layer materials. The results showed that in terms of fatigue performance, plastic geogrid > steel wire mesh > fiberglass > unreinforced specimens. The development of tensile strain can be approximately classified into a three-stage growth pattern, consisting of “curve + straight line + curve”. For the unreinforced specimens, the three stages of bending strain accounted for 10%, 70%, and 20% of the total fatigue life, respectively. The fatigue failure stages of the three types of reinforced materials had similar proportional ranges, representing 5%, 75%, and 20% of the total fatigue life, respectively. The fatigue strain characteristic values for plastic geogrid, steel wire mesh, fiberglass, and unreinforced specimens were 371  $\mu\epsilon$ , 280  $\mu\epsilon$ , 280  $\mu\epsilon$ , and 195  $\mu\epsilon$ , respectively. In summary, the use of reinforced materials within semi-rigid base layers enhances their fatigue performance, providing new insights and methods for extending the service life of road surfaces and offering scientific guidance for the practical application of reinforced materials in semi-rigid base layer road surfaces’ fatigue performance.

**Keywords:** base layer; reinforcement materials; MTS; fatigue performance; spatial stress state

**Citation:** Wang, L.; Zhao, Z.; Liang, H.; He, Y.; Kang, X.; Xu, M. Research on Laboratory Testing Method of Fatigue Performance of Semi-Rigid Base Considering Spatial Stress State. *Buildings* **2024**, *14*, 365. <https://doi.org/10.3390/buildings14020365>

Academic Editor: Hossam El-Din Mohammad Sallam

Received: 21 November 2023

Revised: 22 January 2024

Accepted: 24 January 2024

Published: 29 January 2024



**Copyright:** © 2024 by the authors. Licensee MDPI, Basel, Switzerland. This article is an open access article distributed under the terms and conditions of the Creative Commons Attribution (CC BY) license (<https://creativecommons.org/licenses/by/4.0/>).

## 1. Introduction

Semi-rigid base refers to the base that is paved with inorganic binder-stabilized soil, can form a plate body and has a certain bending strength. Among various pavement structures, semi-rigid base layers have gained widespread application in various construction environments due to their combination of the advantages of both flexible and rigid base layers [1–4]. However, with the continuous increase in traffic volume and load-bearing capacity, many semi-rigid base layer road surfaces still exhibit structural damage, such as fatigue cracking, before reaching their intended service life. This is highly detrimental to the long-term development of pavement structure [5–8]. Therefore, enhancing the fatigue performance of semi-rigid base layers using advanced technology holds significant practical importance [9,10]. The researchers have investigated the effects of structure design [11,12], aggregate types [13,14], cement properties [15–18], and aggregate properties [10,19–21] on the fatigue performance of semi-rigid base layers. The idea that adding reinforcement materials in semi-rigid base layers draws inspiration from the concept of adding reinforcements in bridge structures to improve their flexural tensile performance [22,23]. By enhancing the bond between the reinforcement materials and the base layer materials, the flexural tensile strength and fatigue performance of semi-rigid base layers are improved.

Simultaneously, the occurrence and propagation of cracks in semi-rigid base layer road surfaces are mitigated or suppressed, offering a novel approach to extending road surface service life.

In order to determinate the fatigue failure of semi-rigid base layers accurately, the researchers focused on the influence of environmental conditions [8,24–26], stress intensity [27–29], and vehicle loads [30–33], which provided guidance for the high-performance development of semi-rigid base layers. But these studies also have some shortcomings because they mostly used four-point bending beam specimens to evaluate the fatigue performance of semi-rigid base layers; however, this method only considered unidirectional stress states in small beam specimens under load, while actual road surfaces experience bidirectional stress states under the action of wheel loads. Without accounting for the actual stress states and environmental conditions of road surfaces, the accuracy and reliability of test results are significantly limited. Complex adjustments are necessary in practical design. Therefore, the urgent challenge at hand is to design a new testing method that can simulate the actual spatial stress state in semi-rigid base layers accurately.

To address the issues mentioned above and rectify the considerable disparity between small beam specimen four-point bending fatigue testing methods and the actual stress states and environmental conditions on road surfaces, this paper leverages the Material Test System (MTS) to propose a novel fatigue testing approach that accounts for bidirectional stress states in semi-rigid base-layer road surfaces. Firstly, starting with a mixed design, this paper determines the optimal aggregate grading and prepares reinforced cement-stabilized crushed stone slab specimens. Next, a novel fatigue testing approach is designed to collect fatigue strain data from the specimens, ensuring the reliability and authenticity of the testing process. Finally, through an analysis of specimen fatigue strain, this paper investigates the fatigue failure patterns of semi-rigid base layers and explores the impact of reinforcement factors on the fatigue life, fatigue cracking, and fatigue strain of semi-rigid base layer road surfaces. The results indicate that the indoor testing method for assessing the fatigue performance of semi-rigid base layers, which takes into account spatial stress states, is practical, and that the test data align with theoretical foundations and exhibit a high level of reliability.

## 2. Raw Materials and Mix Design

### 2.1. Raw Materials

#### 2.1.1. Cement

Ordinary Portland cement (Type P·O 42.5) was selected as the cement material. The selection was based on the standards and test procedures outlined in “Common portland cement” (GB 175-2007) [34], “Test Methods of Cement and Concrete for Highway Engineering” (JTG E30-2005) [35], and “Technical Guidelines for Construction of Highway Roadbases” (JTG/T F20-2015) [36]. Relevant tests were conducted to evaluate the performance of the cement material. The test results and performance indicators are presented in Table 1.

**Table 1.** Test Results for Various Parameters of Cement (P·O 42.5).

Test Project	Unit	Index Requirement	Test Result	Test Method
Stability	mm	≤5	2.5	
Setting time	Initial setting time	≥180	330	T 0505—2005
	Final setting time	360~600	400	
Water requirement for standard consistency	%	30.0	28.4	
Specific surface area	m <sup>2</sup> /kg	300~450	380	T 0504—2005
Fineness (80 μm)	%	≤10.0	3.6	T 0502—2005
Density	kg/m <sup>3</sup>	≈3100	3120	T 0503—2005
28 d dry shrinkage	%	≤0.10	0.06	T 0511—2005
Abrasion resistance	kg/m <sup>2</sup>	≤3.0	2.1	T 0510—2005

Table 1. Cont.

Test Project		Unit	Index Requirement	Test Result	Test Method
Flexural strength	3 d	MPa	$\geq 3.5$	4.5	T 0506—2005
	28 d		$\geq 6.5$	9.7	
Compressive strength	3 d	MPa	$\geq 16.0$	21.5	
	28 d		$\geq 42.5$	48.6	

From Table 1, it can be observed that the technical specifications of the Ordinary Portland cement (Type P·O 42.5) comply with the required standards. Therefore, it is suitable for use in fatigue performance testing for reinforced semi-rigid base layer road surfaces.

### 2.1.2. Aggregates

Limestone was used as the aggregate material. In accordance with the “Test Methods of Aggregate for Highway Engineering” (JTG E42-2005) [37] and “Technical Guidelines for Construction of Highway Roadbases” (JTG/T F20-2015) [36], various tests were conducted to evaluate the performance of the aggregates. The test results are presented in Table 2. It is evident that the technical specifications for both coarse and fine aggregates meet the requirements stipulated in the standards.

Table 2. Test Results for Various Parameters of Aggregates.

	Test Project	Unit	Index Requirement	Test Result	Test Method
Coarse aggregate	Crush value	%	$\leq 26$	12.7	T 0316—2005
	Needle flake particle content	%	$\leq 18$	8.2	T 0312—2005
	Dust content below 0.075 mm	%	$\leq 2$	0.7	T 0310—2005
	Soft stone content	%	$\leq 5$	1.3	T 0320—2005
Fine aggregate	Particle analysis	—	Satisfying gradation	Satisfying gradation	T 0327—2005
	Plasticity index	—	$\leq 17$	8.2	T 0118—2007
	Organic matter content	%	$< 2$	0.7	T 0336—1994
	Sulfate content	%	$\leq 0.25$	0.12	T 0341—1994

### 2.1.3. Reinforcement Materials

By referring to the literature, three reinforcing materials, namely selected steel wire mesh, geogrid and glass fiber, which have been mentioned many times, were selected, and then, combined with factors such as material acquisition difficulty and raw material price, galvanized steel wire mesh, biaxial plastic geogrid and glass fiber geogrid were finally selected as reinforcing materials in this paper.

#### (1) Galvanized Steel Wire Mesh

As shown in Figure 1, galvanized steel wire mesh with 3 cm openings and a 0.7 mm wire diameter was chosen as the reinforcement material. Performance tests of the galvanized steel wire mesh were conducted based on “Welded wire fabric coated with zinc” (GB/T 33281-2016) [38], “Test method for gravimetric determination of the mass per unit area of galvanized coatings on steel products” (GB/T 1839-2008) [39], and “Metallic materials—Tensile testing—Part 1: Method of test at room temperature” (GB/T 228.1-2021) [40]. The test results and performance indicators are presented in Table 3.

#### (2) Biaxial Plastic Geogrid

As shown in Figure 2, polypropylene biaxial plastic geogrid with a designation of TGSG50-50 was selected as the reinforcement material. Performance tests of the biaxial plastic geogrid were carried out based on “Geosynthetics—Plastic geogrids” (GB/T 17689-2008) [41]. The test results and performance indicators can be found in Table 3.



Figure 1. Galvanized Steel Wire Mesh.

Table 3. Test Results of Various Parameters for Reinforcement Materials.

Reinforcement Materials	Test Project	Unit	Index Requirement	Test Result	Test Method
Galvanized Steel Wire Mesh	Diameter	mm	$0.70 \pm 0.04$	0.69	
	Warp mesh size (clear)	mm	$30.00 \pm 0.75$	30.22	GB/T 33281-2016 [38]
	Weft mesh size (clear)	mm	$30.00 \pm 0.30$	30.15	GB/T 1839-2008 [39]
	Solder joint tensile force	N	>40	118	GB/T 228.1-2021 [40]
	Zinc layer quality	g/m <sup>2</sup>	>122	161	
Bidirectional Plastic Geogrid	Ultimate tensile strength	Portrait	≥50.0	51.9	GB/T 17689-2008 [41]
		Landscape orientation	≥50.0	51.6	
	Elongation at nominal strength	Portrait	≤15.0	13.7	
		Landscape orientation	≤13.0	12.9	
	Tensile strength at 2% elongation	Portrait	≥17.5	18.4	
		Landscape orientation	≥17.5	18.6	
	Tensile strength at 5% elongation	Portrait	≥35.0	35.3	
	Landscape orientation	≥35.0	35.7		
Glass Fiber Geogrid	Meridional fracture strength	kN/m	≥50.0	51.7	GB/T 21825-2008 [42]
	Zonal breaking strength	kN/m	≥50.0	51.2	
	Elongation at break	%	≤4.0	2.5	
	Elongation at zonal break	%	≤4.0	2.6	



Figure 2. Biaxial Plastic Geogrid.

### (3) Glass Fiber Geogrid

As shown in Figure 3, a glass fiber geogrid with a designation of EGA50-50 was chosen as the reinforcement material. Performance tests of the glass fiber geogrid were conducted based on “Glass fibre geogrid” (GB/T 21825-2008) [42]. The test results and performance indicators are presented in Table 3.



**Figure 3.** Glass Fiber Geogrid.

From Table 3, it is evident that the technical specifications of the galvanized steel wire mesh, biaxial plastic geogrid, and glass fiber geogrid all meet the required standards. Therefore, they can be used in fatigue performance testing for reinforced semi-rigid base layer road surfaces.

## 2.2. Mix Design

### 2.2.1. Aggregate Grading Design

Various aggregates were subjected to sieve analysis in accordance with the “Test Code for Highway Engineering Aggregates” (JTG E42-2005). The mix design for aggregates was selected based on the “Technical Specifications for Road Base Construction” (JTG/T F20-2015). For the semi-rigid base layer material, cement-stabilized crushed stone was chosen, and the mix design selected followed the recommended C-B-1 type as per the specifications. The aggregate grading curve is shown in Figure 4.

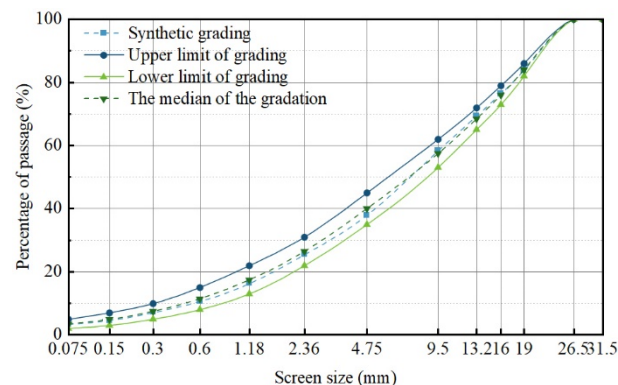


**Figure 4.** Gradation Curve of Aggregate.

Taking into consideration the recommended aggregate grading range and practical experience in aggregate design, after repeated calculations and comparisons, the optimal aggregate ratio for various particle sizes was determined to be 20 mm~30 mm:10 mm~20 mm:5 mm~10 mm:0 mm~5 mm = 18:34:17:31.

### 2.2.2. Optimal Moisture Content

For cement-stabilized materials, cement dosages of 3%, 4%, 5%, 6%, and 7% were considered, and external water was used. Moisture content levels of 4%, 4.5%, 5%, 5.5%, 6%, and 6.5% were evaluated. A heavy-impact compaction test was conducted on the cement-stabilized crushed stone mixture prepared in the determined proportions to establish the optimal moisture content. Additionally, the unconfined compressive strength at 7 days was measured. The results are illustrated in Figure 5.

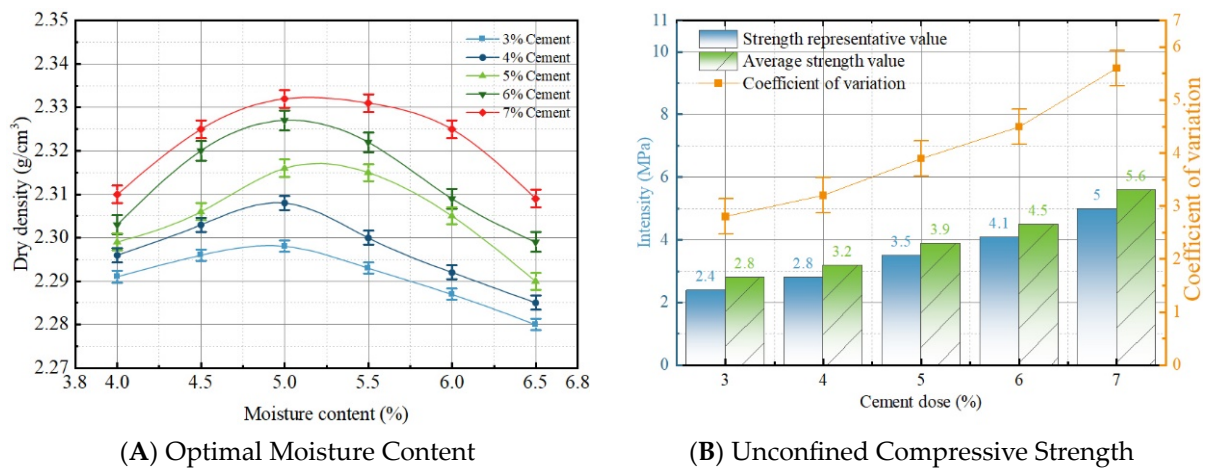


**Figure 5.** Optimal Moisture Content and Unconfined Compressive Strength.

The representative value of unconfined compressive strength should meet or exceed the strength standard values. Considering the relatively high market price of cement, and while prioritizing cost-effective solutions that ensure project quality in practical engineering, a cement dosage of 5% was selected along with a moisture content of 5.2% and a maximum dry density of 2.318 g/cm<sup>3</sup>. These parameters were chosen based on both design and construction experience. The combination of these values was deemed suitable for the project. To validate the technical performance of the synthetic graded mixture, it was confirmed that the strength requirements were met, and the mixture exhibited good resistance to erosion and cracking.

### 2.3. Specimen Preparation

Specimen preparation methods drew from the techniques used for inorganic binder-stabilized material beam specimens. The mold for specimen molding was inspired by the rutting plates used in asphalt mixture rutting tests, with enhancements such as increased height and thickness. The dimensions are as shown in Figure 6 (inner dimensions designed as 300 mm × 300 mm × 100 mm). The molding process is illustrated in Figure 6.



**Figure 6.** Specimen Preparation Flowchart.

Due to the large number of specimens required for the experiments, a small mixer, as shown in Figure 6, was chosen for mixing. Unreinforced specimens were selected as the reference group. Different specimens were molded after the placement of reinforcement materials and were finally statically compacted. According to the testing protocol, specimens were cured after demolding, with a 90-day curing period and water immersion treatment on the final day. Given the significant time span of specimen preparation, large temperature variations, and substantial material requirements, it was deemed necessary to increase the number of specimens to ensure the accuracy of the experiments. Additionally, the selection of the stress ratio directly affects the results of fatigue testing. After considering various factors, three stress ratios (0.5, 0.6, 0.7) were chosen as the test loads, and the number of specimens prepared is outlined in Table 4.

**Table 4.** Number of Specimens Prepared.

Type of Reinforcement	Stress Ratio	Test Quantity	Reserve Quantity
Unreinforced	0.5, 0.6, 0.7	$3 \times 10 = 30$	$3 \times 2 = 6$
Wire mesh	0.5, 0.6, 0.7	$3 \times 5 = 15$	$3 \times 1 = 3$
Biaxial plastic geogrid	0.5, 0.6, 0.7	$3 \times 5 = 15$	$3 \times 1 = 3$
Glass fiber grille	0.5, 0.6, 0.7	$3 \times 5 = 15$	$3 \times 1 = 3$

### 3. Test Method

Currently, there are two main types of test methods for studying the fatigue performance of road surfaces. One type of method involves subjecting real vehicle loads to actual road surfaces for fatigue testing or using large-scale full-scale testing to simulate fatigue experiments [43–45]. These methods are advantageous in that they can better reflect the real fatigue performance of road surfaces. However, they are costly and time-consuming, and the test results are significantly influenced by the environment and road structure. Therefore, these methods are less commonly used and are not suitable for current research on the fatigue performance of semi-rigid road surfaces. The other type of method primarily involves indoor small-scale fatigue testing. Currently, the four-point bending beam fatigue test method is the most commonly used. However, this method results in a uniaxial stress state in the beam specimen under load, whereas actual road surfaces experience complex spatial stress states under the action of vehicle wheels. As a result, the accuracy and reliability of test results are greatly limited, as it does not consider the actual stress states and environmental effects on the road surface. To address the issue of the mismatch between the four-point bending fatigue test method and the actual stress state, this paper presents a two-way stress-bearing fatigue test method for semi-rigid base-layer road surfaces based on the Material Test System (MTS) material testing system.

#### 3.1. Fatigue Test Loading Device

The fatigue loading test utilizes the MTS 810 material testing system. The system comprises a load frame with a loading head connected to it. A hydraulic oil source is connected to the load frame to provide pressure, and a control system is linked to the load frame to control the loading mode on the specimen.

The design of the loading head was inspired by the testing wheel of the rutting tester. The testing wheel has an outer diameter of 200 mm and a width of 50 mm, with the tire made of high-strength rubber. The loading head features multiple bolt holes, and the actuator head is securely fixed to the loading head using several bolts and bolt holes. The loading head's structure, which includes the testing wheel, can be used to apply load to the specimens, effectively simulating the load conditions that road surfaces experience when vehicles are driven over them.

At the beginning of the test, turn on the hydraulic oil source and compressor of the MTS material test device to check whether the mechanical equipment and power supply of the test system are normal. The driving rod on the beam is adjusted to the appropriate length, and the acting head is installed on the driving rod through a large bolt, and adjusted

to the appropriate position above the specimen. The loading head is installed on the acting head by small bolts, and the upper surface of the loading head is horizontal. The connection lines of the stress sensor and displacement sensor on the computer are connected to the test device to set the loading mode. The beam is controlled by the load frame control unit to make the loading head just contact with the upper surface of the specimen.

Before the test, the corresponding operation is carried out through the control windows on the software, such as assigning sensors, setting limits, clearing sensors, setting error limits, adjusting parameters, etc., and the relevant test program is compiled. After repeated debugging to reliable and stable, can be carried out formal test.

The fatigue test was conducted under stress control mode, the loading waveform was half sine wave, and the load frequency was 10 Hz. The test time was relatively short under the stress control mode, the failure was clearly defined, and the complete fracture was the failure, which was more consistent with the actual stress condition of the structure layer.

In order to protect the test equipment, the procedure shall specify the relevant protection procedure for the termination of the test. In the process of test loading, the output data of the sensor is recorded. When the number of loading times is reached or the surface structure of the specimen is damaged, the loading is stopped. By lifting control of the drive rod, the loading head is lifted upward, the damaged specimen is removed, and the other specimen is placed to continue the above test. After a batch of samples is completed or all tests are completed for the day, the obtained data will be stored.

### 3.2. Fatigue Failure Ultimate Load

The flexural ultimate load test not only determines the failure ultimate load of cement-stabilized crushed stone materials, but also provides the basic parameters for load application standards. The data acquisition process is illustrated in Figure 7A. The flexural ultimate load test on unreinforced slab specimens was conducted using a load applied at the center point of the testing wheel, and the maximum load at which the center point of the specimen failed is defined as the ultimate failure load. The center point of the specimen failed, as shown in Figure 7B. The flexural ultimate load of the cement-stabilized crushed stone slab was found to be 12.31 kN.

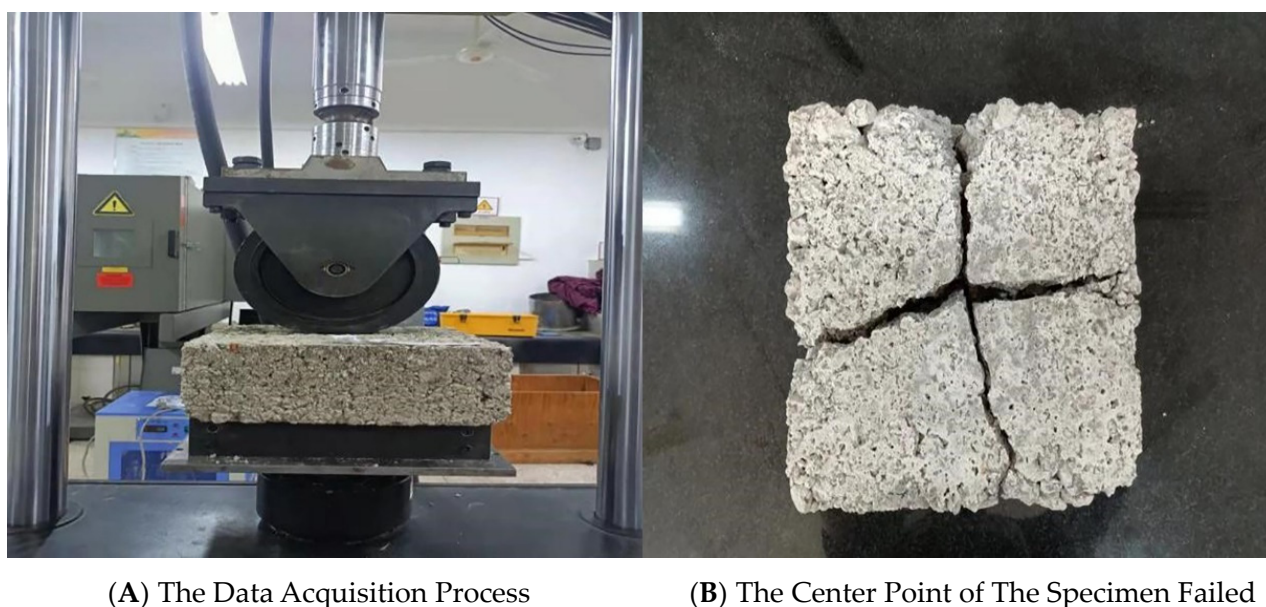


**Figure 7.** Specimen Failure States.

### 3.3. Supportive Fatigue Test Method

In conventional indoor bending fatigue tests, beam specimens are subjected to loading in a simply supported state without any support. Typically, the specimens fracture instantly,

making it difficult for observers to carefully observe the crack formation before the complete failure. In actual road surface structures, there is often a supportive layer like a subbase or subgrade beneath the semi-rigid base layer. The presence of this layer significantly delays crack propagation at the bottom of the base layer, allowing the base layer to maintain its integrity and function normally for an extended period.

### 3.3.1. Supportive Material

To better simulate the real stress conditions of road surface structures, suitable supportive materials were selected and placed at the bottom of the cement-stabilized crushed stone slab specimens during the experiments. These materials were chosen to emulate the supporting layer in actual road surface structures, providing resistance to compression, distributing loads, and reducing deformation. Four materials, as shown in Figure 8, were considered, with the elastic modulus as a crucial parameter for the supportive material. Based on the experimentally determined elastic modulus of typical supportive layers in semi-rigid base layers, which generally falls within the range of 300 MPa to 500 MPa, and considering the technical specifications of different support materials, rubber sheets were found to best meet the experimental requirements for supportive material.

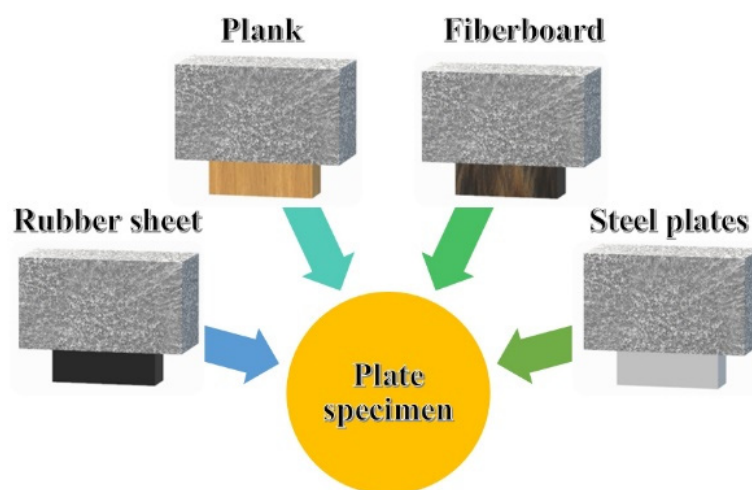


**Figure 8.** Plate Support Material.

### 3.3.2. Support Method for Specimens

The experimental support method involves central contact, ensuring that the slab specimen is in close contact with the rubber sheet while also making direct contact with the lower fixture base to facilitate bending fatigue testing under support conditions.

The dimensions of the rubber sheet are 200 mm × 200 mm × 50 mm, and its compressive elastic modulus meets the requirements. The total height of the supportive material is adjusted by adding or removing 1 mm thick rubber sheets to ensure close contact between the supportive material and the slab specimen.

### 3.3.3. Fatigue Strain Testing of Specimens

To visually summarize the development of fatigue strain in the reinforced semi-rigid base layers, strain gauges were used to measure the stress, load-carrying capacity, and fatigue performance of the reinforced cement-stabilized crushed stone slab under loading conditions. The strain gauge was attached to the center of the lower surface of the cement-stabilized crushed stone plate specimen. When a load was applied to the specimen, it deformed, causing the strain gauges to deform in tandem, resulting in changes in their resistance values. The resistance strain measurement device was capable of measuring these changes, converting them into strain values, or outputting analog signals proportional to strain. After data collection and processing with a computer, the required strain values

were obtained. The strain measurement device and resistance strain gauges used in this study are shown in Figure 9.

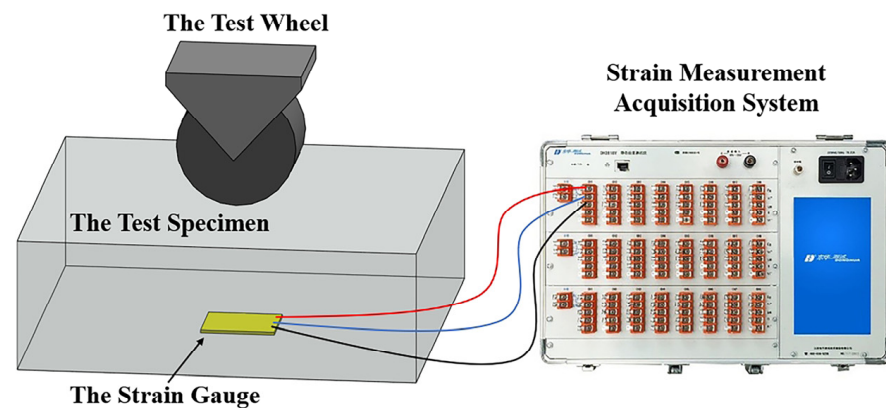


**Figure 9.** Strain Measurement Device and Resistance Strain Gauge.

Prior to the start of the experiment, strain gauges were attached to the central position on the lower surface of the cement-stabilized crushed stone slab specimens. Once the experimental setup was complete, the loading head was lowered until it made contact with the specimen. The MTS fatigue test system and strain measurement acquisition system were then initiated. The fatigue test was conducted in stress control mode, utilizing a half-sine wave waveform with a load frequency of 10 Hz, which closely matched the stress conditions of actual structural layers. As illustrated in Figure 10, fatigue strain data were collected during the test.



**Figure 10.** Fatigue Strain Test Data Acquisition System.

#### 4. Analysis of Fatigue Cracking Characteristics of Stiffened Water Stabilizer Plate

The fatigue cracking of semi-rigid base pavement mostly starts from the fatigue cracking of base pavement. Under the continuous action of load, the cracks extend to the asphalt surface, causing fatigue cracking of the whole pavement and fatigue failure of the pavement. When the bearing fatigue test method is used to test the cement stable broken slate specimen, because there are supports at the bottom of the specimen, the crack of the specimen will not break quickly in a short time after the crack appears, and the

process from crack appearance to complete fracture lasts a long time, so the crack cracking condition of the specimen can be closely observed.

Most cracks appear in the bottom of the specimen with pores, segregation and other defects, and continue to expand along the long axis of the initial crack. Among them, the two-directional tensile stress at the center of the plate specimen is basically the same. When the two-directional stress  $\sigma_x = \sigma_y$ , axial symmetry within a certain range is formed locally, and the maximum tensile stress in each direction is the same. At this time, cracking may occur in any direction.

As the number of fatigue loads continues to increase, multiple cracks in different directions begin to connect, forming cracks with a certain length, and the crack length gradually increases. When the crack length approaches the length of the specimen, one or more main cracks will be formed through the center of the bottom of the specimen. After the formation of the main crack, the width of the crack gradually increases, and it can be clearly observed from the side of the specimen that the main crack develops from bottom to top, the deflection of the specimen changes, the stiffness of the specimen decreases sharply, and finally the specimen is completely cracked and destroyed.

The fatigue cracking of cement-stabilized broken slate specimens has the following characteristics: (1) The crack is mainly caused by the original defects at the bottom of the specimen, and the crack distribution in the center of the specimen is multi-directional and finally forms different bottom cracks. (2) Before the formation of the main crack of the specimen, the length and width of the crack of the specimen develop slowly, and after the formation of the main crack of the specimen, the length and width of the crack of the specimen develop more rapidly. (3) There will be a number of cracks at the bottom of the specimen; the depth of the crack surface at the center is the largest, when the crack expands from the bottom to the bottom, the length of the crack at the bottom of the specimen develops at the same time; and when a crack develops to the surface of the specimen, the specimen will be completely cracked, and the width of the crack at the surface position of the specimen is less than the bottom position of the specimen.

## 5. Test Results and Analysis

The fatigue strain of semi-rigid base layer materials is primarily composed of elastic strain and plastic strain. The degree of fatigue damage can be represented by the fatigue strain peak value, which corresponds to the maximum strain value under cyclic loading. Under the continuous action of cyclic loading, the material experiences elastic degradation and plastic accumulation failure. The maximum stress is constant at all stress ratios, so the effect of fatigue strain on the specimen is only caused by cyclic loading. When the stress level is high, both elastic and plastic strains develop rapidly, leading to a quick increase in elastic degradation and plastic accumulation, resulting in a shorter fatigue life. When the stress level is low, most of the fatigue strain is elastic, with a lesser contribution from plastic strain, which significantly extends the fatigue life.

### 5.1. Analysis of Fatigue Strain Growth Patterns of Specimens with Different Reinforcement Materials

Taking the fatigue life and strain values under a stress ratio of 0.5 from Figure 11 as an example, the fatigue failure of the specimens can be mainly divided into three stages, corresponding to the three magnified parts A, B and C in the Figure 11. Combining the fatigue failure mechanism of semi-rigid base layers and actual observations [46–48], the characteristics of these three stages are as follows:

**First Stage:** The MTS testing machine head closely contacts the specimen, and at the beginning of the test, the strain at the bottom of the specimen increases rapidly and is unstable. After a short period of fluctuation, the tensile strain values start to increase more slowly and stabilize.

Second Stage: Most of the strain in the specimen is elastic strain. The strain peak value at the bottom of the specimen increases relatively slowly, and the rate of increase approaches a certain value, approximately in linear relation to the number of fatigue cycles.

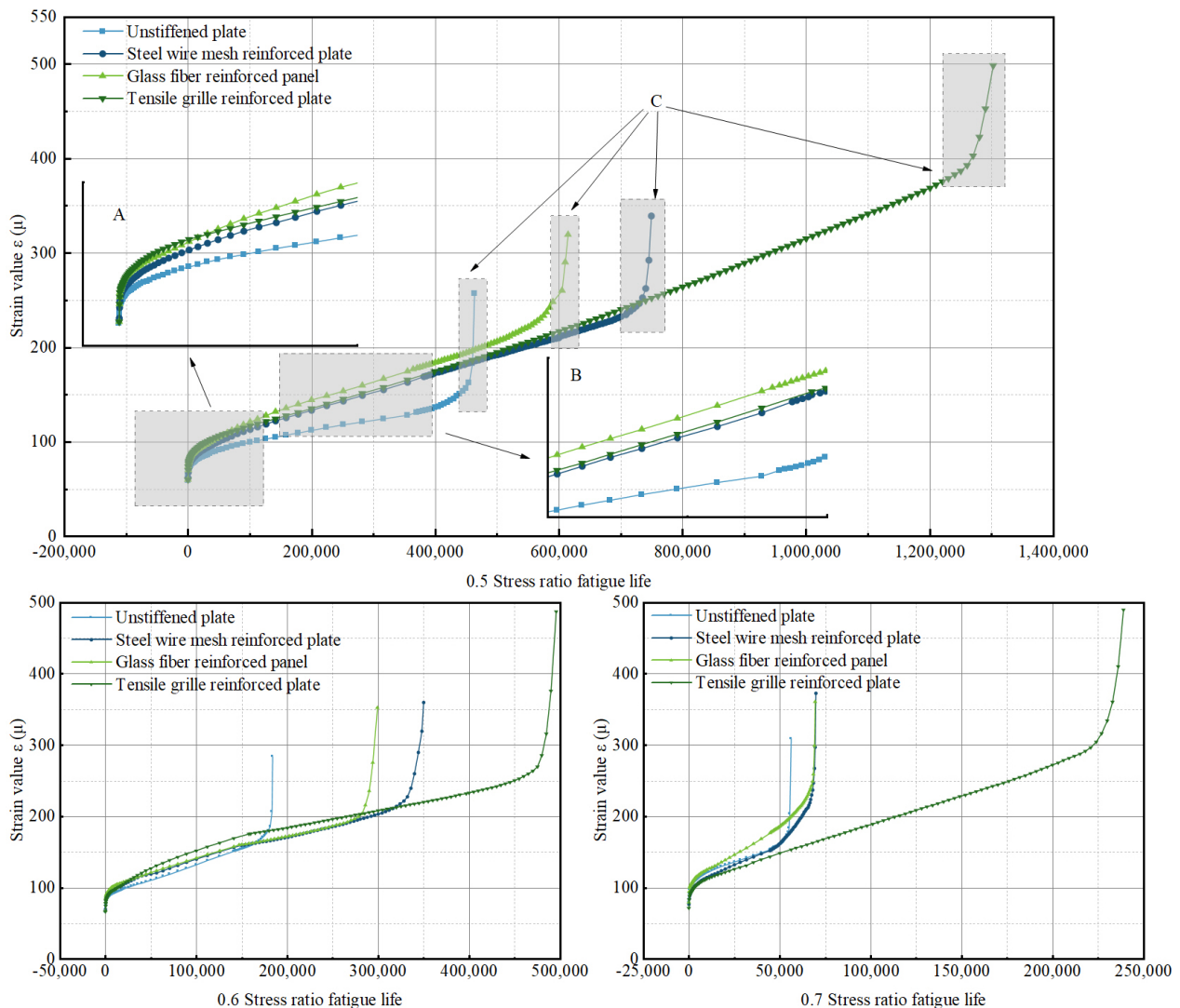


**Figure 11.** Strain Development Behavior of Specimens.

Third Stage: With an increasing number of cyclic loading cycles, plastic strain starts to increase. The strain peak value in the specimen increases rapidly and reaches the limit tensile strain, resulting in fatigue fracture and failure within a relatively short time.

A comprehensive analysis of Figure 11 reveals that reinforced materials exhibit better fatigue resistance compared to unreinforced materials. Among the reinforced materials, the geogrid reinforcement shows relatively good performance. Across different stress ratios, the fatigue life of specimens consistently follows this order: pull-plastic grid > steel wire mesh > fiberglass > unreinforced. The main reason is that the technical performance of the three kinds of reinforced materials is different. From the technical parameters and actual use of the three kinds of reinforced materials, the tensile strength, hardness and elongation of the pull-plastic grid is superior to those of the steel wire mesh and the glass fiber grid in many aspects, and the tensile grid has better bonding performance with the cement stabilized gravel. The pull-plastic grid forms an effective bearing and diffusion chain system in the cement stabilized gravel, increases the bearing capacity of the pavement base, and extends its service life. The strength of the glass fiber grating is lower than that of the pull-plastic grid, the elongation is also lower, and the bonding performance of the cement stabilized

gravel material is general, but the glass fiber grating has a better bonding performance with the asphalt mixture, and the resistance effect of high temperature rutting in the asphalt pavement is better. The strength of the steel wire mesh is between the pull-plastic grid and the glass fiber grid, the elongation is also low, and the bonding performance of the cement-stabilized gravel material is good, but the steel wire mesh is easy to rust in the wet environment, resulting in its tensile strength gradually reduced, and the fracture failure occurs under the continuous action of load. Analyzing the proportion of fatigue life in each stage based on the three-stage fatigue failure analysis, for unreinforced specimens, the first stage accounts for 10% of the total fatigue life, the second stage accounts for 70%, and the third stage accounts for 20%. Similarly, for the other reinforced specimens, the analysis indicates that the proportions of fatigue failure in the three stages are consistent, at 5%, 75%, and 20% of the total fatigue life. This suggests that the inclusion of reinforcement materials accelerates the entry of the specimens into the elastic failure stage, thereby extending their fatigue life.

### 5.2. Analysis of Fatigue Strain Growth Patterns for Specimens under Different Stress Ratios

Analysis of fatigue strain values for different specimens under different stress ratios, as shown in Figure 12, reveals that reinforced specimens consistently exhibit better fatigue resistance compared to unreinforced ones at varying stress ratios. Stress levels have a significant impact on strain development, with higher stress ratios leading to greater strain growth rates. In terms of initial strain values, it is evident that all specimens at high stress ratios have significantly higher initial values than those at low stress ratios. Analyzing the strain growth rates, it becomes apparent that in reinforced specimens, the strain growth rates during the second and third stages are notably higher at high stress ratios compared to low stress ratios. Strain development during the second and third stages of reinforced specimens shows a linear relationship with the number of loading cycles, with the strain growth rate during the third stage being higher than that during the second stage.

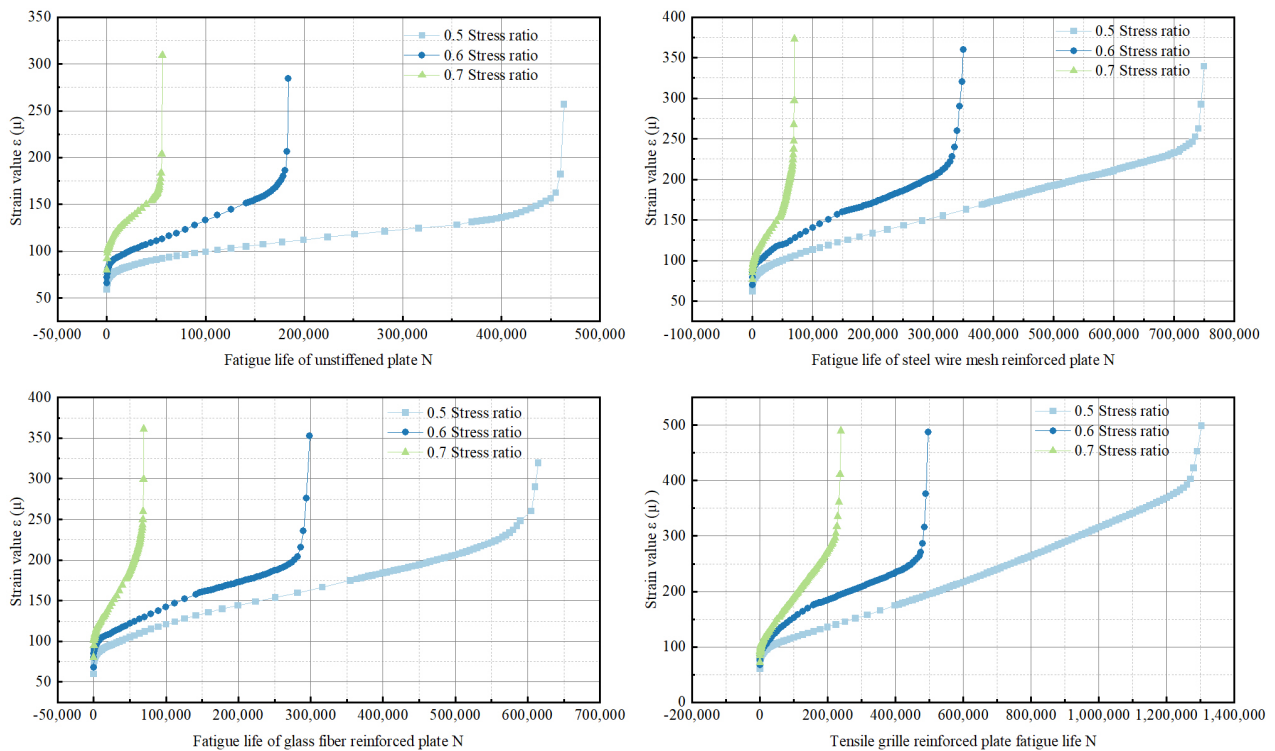


**Figure 12.** Changes in Strain Characteristics under Different Stress Levels for Specimens.

### 5.3. Analysis of Fatigue Strain Characteristics

In the context of the novel supporting fatigue test designed in this study, the use of characteristic values to represent critical points of fatigue strain-related to the various stages of fatigue failure was considered. Comparative analysis revealed variations in the initial tensile strain and tensile strain growth patterns of cement-stabilized crushed stone slabs reinforced with different materials and under different stress levels. By examining the fatigue strain development curves of reinforced specimens and the fatigue failure mechanism of semi-rigid base layers, a regression analysis was conducted to determine the initial strain value, strain inflection point, and ultimate strain value for different reinforced specimens.

Taking the example of the pull-plastic grid, which exhibits the best fatigue resistance, its tensile strain development pattern shows stage-wise changes. The tensile strain development in the first and third stages appears to follow a curve, while the second stage demonstrates linear strain growth. A linear regression analysis was performed on the tensile strain development during the second stage. The point at which the linear regression intersects with the curve in the third stage represents the tensile strain inflection point, and the point of abrupt change in the curve during the third stage indicates the ultimate tensile strain point.

With respect to the varying stress ratios, the analysis of strain characteristic values in Figure 13 reveals the following: at a stress ratio of 0.5, the reinforced panel with pull-plastic grid exhibits an initial strain value of approximately  $79 \mu\epsilon$ , a tensile strain inflection point of approximately  $228 \mu\epsilon$ , and an ultimate tensile strain value of about  $453 \mu\epsilon$ . At a stress ratio of 0.6, the initial strain value is approximately  $82 \mu\epsilon$ , the tensile strain inflection point is about  $196 \mu\epsilon$ , and the ultimate tensile strain value is roughly  $316 \mu\epsilon$ . At a stress ratio of 0.7, the initial strain value is around  $72 \mu\epsilon$ , the tensile strain inflection point is approximately  $209 \mu\epsilon$ , and the ultimate tensile strain value is about  $360 \mu\epsilon$ . In summary, the strain characteristic values align with the theoretical foundations of fatigue failure, effectively representing the three stages of semi-rigid fatigue failure mechanisms, and they offer a representative assessment of the extent of fatigue failure for the specimens. Additional characteristic values for other specimens are provided in Table 5.

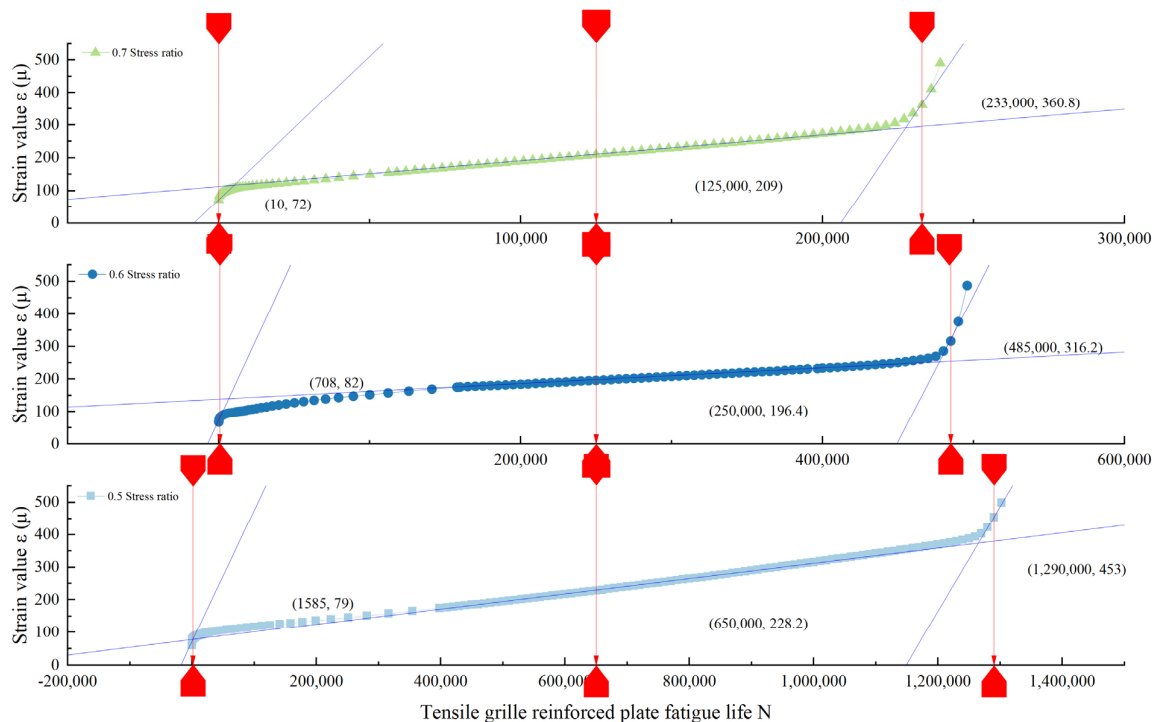


**Figure 13.** Changes in Strain Characteristics of Pull Plastic Geogrid Specimens under Different Stress Ratios.

**Table 5.** Strain Characteristics under Different Stress Ratios for Various Reinforced Plates.

Material Type	Stress Ratio	Strain Value ( $\mu\epsilon$ )		
		Initial Strain Value	Turning Point of Strain	Ultimate Tensile Strain Value
Unstiffened plate	0.5	72	153	182
	0.6	83	176	196
	0.7	101	171	203
Steel wire mesh reinforced plate	0.5	77	170	272
	0.6	90	161	290
	0.7	98	155	277
Tensile grille reinforced plate	0.5	79	228	453
	0.6	82	196	316
	0.7	72	209	360
Glass fiber grid reinforced panel	0.5	81	177	265
	0.6	92	160	276
	0.7	108	175	280

## 6. Conclusions

This study proposed a novel fatigue testing method for semi-rigid base layer road surfaces based on MTS, which simulates bidirectional stress conditions. By preparing reinforced cement-stabilized crushed stone slab specimens and conducting indoor fatigue strain tests, the study explored the impact of reinforcement factors on fatigue strain in semi-rigid base layers. It provides an experimental foundation for the practical application of reinforcing materials in semi-rigid base layer road surfaces. Compared with the current fatigue test method, which mainly adopts the four-point bending beam fatigue test method, the unidirectional stress state of the beam specimen under load is changed to the bidirectional stress state of the actual road surface under the action of the wheel, the authenticity of the test results is improved, the accuracy and reliability are guaranteed, and the complicated correction in the actual design is simplified. The main conclusions are as follows:

- The strain growth rate in semi-rigid base layers is directly proportional to the stress ratio, and reinforced specimens consistently exhibit better fatigue resistance than unreinforced specimens. When comparing different reinforcing materials for their fatigue resistance, it is evident that they perform as follows: pull-plastic grid > steel wire mesh > glass fiber > unreinforced specimens.
- The failure of semi-rigid base layers can be primarily divided into three stages, with corresponding strain changes approximated as a combination of curved, linear, and curved changes. For unreinforced specimens, the proportions of fatigue life in each stage are 10%, 70%, and 20%. The addition of reinforcement materials prolongs the elastic failure stage of semi-rigid base layers and enhances their fatigue life, with proportions of fatigue life in each stage reaching 5%, 75%, and 20%.
- Using characteristic strain values to represent the extent of fatigue failure in the novel support fatigue test satisfies the theoretical foundations of fatigue failure. It effectively represents the three stages of semi-rigid base layer fatigue failure mechanisms, providing a representative assessment of the extent of fatigue failure for the specimens.

**Author Contributions:** Conceptualization, L.W. and Z.Z.; methodology, L.W., H.L., Y.H. and X.K.; software, M.X.; formal analysis, X.K.; investigation, L.W. and Z.Z.; resources, X.K.; data curation, L.W., Z.Z., Y.H. and X.K.; writing—original draft preparation, Z.Z. and Y.H.; writing—review and editing, L.W. and M.X.; visualization, H.L. and M.X.; supervision, H.L., Y.H. and M.X.; project administration, Y.H. and M.X.; funding acquisition, M.X. All authors have read and agreed to the published version of the manuscript.

**Funding:** This study is supported by the National Key R&D Program of China (2022YFB2601900), National Natural Science Foundation of China (U2233210 and 51978034), the Beijing Scholars Foundation (No. 067), the Beijing Natural Science Foundation, the Beijing Municipal Education Commission (KZ202110016020) and the Shandong Jiaotong University Scientific Research Fund Project (23YK029).

**Data Availability Statement:** The raw data supporting the conclusions of this article will be made available by the authors on request.

**Conflicts of Interest:** Author Hao Liang was employed by the Shandong Luzhong Highway Construction Co., Ltd. Author Yilong He was employed by the Shandong Expressway Environmental Protection Building Materials Co., Ltd. The remaining authors declare that the research was conducted in the absence of any commercial or financial relationships that could be construed as a potential conflict of interest.

## References

1. Cao, J.; Zhang, B. Study on long-term performance of four types of asphalt pavement with different base layers. *Highway* **2020**, *65*, 1–665.
2. Shen, W.; Zheng, X.; Li, H. Classification and service status of pavement base materials. *J. Wuhan Univ. Technol.* **2021**, *43*, 1–5.
3. Tang, Y.; Zhang, K. Analysis on the Fatigue Properties of Semi-Rigid Base Asphalt-Pavement Structures With Horizontal Interfacial Cracks. *J. Test. Eval.* **2017**, *45*, 20160091. [[CrossRef](#)]
4. Jia, W.; Hu, M.; Liu, Z.; Li, T.; Chen, S.; Gao, J. Experimental Study on Interlayer Mechanical Properties of Semi-Rigid Base Asphalt Pavement Using Interlayer Treatment Method. In *IOP Conference Series: Earth and Environmental Science*; IOP Publishing: Bristol, UK, 2021; Volume 719, pp. 32070–32075.
5. Guo, F. Analysis and Research on Fatigue Characteristics of Semi-Rigid Base Layer of Permanent Pavement. Master's Thesis, Chongqing Jiaotong University, Chongqing, China, 2023.
6. Wang, L. Numerical Simulation Analysis of Mechanical Effects on Long-Life Pavement under Semi-Rigid Base Mode. Master's Thesis, Jilin University, Changchun, China, 2022.
7. Jia, K. Research on Fatigue Characteristics of Semi-Rigid Base Materials. Master's Thesis, Chang'an University, Xi'an, China, 2008.
8. Wang, L.; Lei, X.; Liu, S. Investigation of immersion influence on dynamic properties of high-speed railway subgrade with semi-rigid waterproof functional layer through field-excitation testing. *Can. Geotech. J.* **2017**, *55*, 19–33. [[CrossRef](#)]
9. Song, Y.; Jin, M.; Qiu, H. Alkali excitation slag recycled aggregate semi-rigid base. *J. Mater. Sci. Eng.* **2023**, *9*, 455–461.
10. Lv, S.; Hu, L.; Peng, X.; Cabrera, M.B.; Li, J. Investigation of structural resistance for semi-rigid layers in an actual stress state. *Constr. Build. Mater.* **2021**, *273*, 122041. [[CrossRef](#)]
11. Wang, X.; Huang, X.; Bian, G. Reflection crack propagation path analysis of semi-rigid base asphalt pavement based on numerical simulation. *Highway* **2018**, *63*, 1–6.
12. Liu, J. Structural design analysis of semi-rigid asphalt pavement on highways. *Transp. Manag. World* **2023**, *21*, 34–36.
13. Zhang, Z. Research on semi-rigid base materials and structural fatigue damage of asphalt pavement. *Zhonghua Constr.* **2023**, *10*, 154–156.
14. Zhu, Y. Research on Design Control Index of Semi-Rigid Base Asphalt Pavement. Master's Thesis, Southeast University, Nanjing, China, 2019.
15. Liu, J. Study on Design Index and Road Performance of Chinese-French Asphalt Concrete and Semi-Rigid Base Material. Master's Thesis, Highway Science Research Institute of the Ministry of Transport, Beijing, China, 2019.
16. Zhao, G. Effect of high dosage of cement on performance of cement-stabilized gravel base. *China Munic. Eng.* **2019**, *06*, 92–95+109.
17. Busch, C.; Th Gersen, F.; Henrichsen, A. Development and Validation of a Mechanistic Recursive-Incremental Deterioration Model for Cement-Stabilized Base Courses. *Transp. Res. Rec.* **2018**, *1974*, 128–137. [[CrossRef](#)]
18. Zhang, B.; Zhang, X.; Zhong, Y.; Li, X.; Hao, M.; Sang, X.; Wang, X.; Liu, J. Research on Fatigue Model of Semi-Rigid Base Asphalt Pavement before and after Polymer Grouting. *Adv. Civ. Eng.* **2021**, *2021*, 6658943. [[CrossRef](#)]
19. Mohammadinia, A.; Disfani, M.M.; Narsilio, G.; Hemachandra, P.; Aye, L. Application of semi-rigid composite permeable pavements in road network. *Geotech. Innov. Chall. Transp. Infrastruct.* **2017**, 119–126.
20. Tian, X. Research on the Cracking Process and Influencing Factors of Regenerated Semi Rigid Base. Master's Thesis, Shaoxing University of Arts and Sciences, Shaoxing, China, 2023. [[CrossRef](#)]
21. Yu, L.; Pei, J.; Li, R. Research on Maintenance Strategies and Benefits of Semi rigid Base Crushed Petrochemical. In *Chinese Association for Science and Technology, Ministry of Transport, Chinese Academy of Engineering, Hubei Provincial People's Government. 2022 World Transportation Conference (WTC2022) Paper Collection (Highway Engineering)*; China Communication Press: Beijing, China, 2022; p. 6. [[CrossRef](#)]
22. Peng, T.; Gong, S.; Zhu, Y. Research on the Performance of Reinforced Soil Abutment Composite Structures under Static Load. In *Chinese Association for Science and Technology, Ministry of Transportation, Chinese Academy of Engineering, Hubei Provincial People's Government. Proceedings of the World Transportation Congress (WTC2022) (Bridge and Tunnel Engineering)*; China Communication Press: Beijing, China, 2022; p. 9.
23. González, M.; Villalobos, F.; Méndez, A.; Carrillo, P. Study of the static and seismic performance of a geogrid reinforced soil wall as bridge abutment in Concepción. *Obras Y Proy.* **2018**, *24*, 41–52. [[CrossRef](#)]
24. Zhang, H.; Zang, G.; Wu, B. Simulation analysis of dynamic strain response of semi-rigid base asphalt pavement. *Transp. Sci. Technol.* **2017**, *5*, 65–67.

25. Jin, F. Damage Characteristics and Service State Evaluation of Semi-Rigid Base. Master's Thesis, Harbin Institute of Technology, Harbin, China, 2020. [[CrossRef](#)]
26. Li, X. Stress analysis and treatment method of reflection crack in semi-rigid base road under temperature action. *Highway* **2017**, *62*, 54–60.
27. Li, S.; Sun, P.; Sun, T.; Nie, D.; Wang, D. Fatigue life analysis of semi-rigid base pavement based on three-dimensional scale variation of hidden cracks. *Highway* **2014**, *59*, 61–69.
28. Sun, R. Research on Reinforcement Effect and Application Technology of Geogrates in Widening Highway. Master's Thesis, Shandong University, Jinan, China, 2018.
29. Gao, Y. Theoretical Analysis of Reflective Cracking in Asphalt Pavement with Semi-rigid Base. *Iran. J. Sci. Technol. Trans. Civ. Eng.* **2019**, *43*, S149–S157. [[CrossRef](#)]
30. Huang, L.; Song, W.; Jiang, Z.; Yang, S. The influence of temperature and vehicle speed on the modulus field and fatigue life of semi-rigid base asphalt pavement. *J. Hunan Univ. (Nat. Sci. Ed.)* **2021**, *48*, 148–156. [[CrossRef](#)]
31. Yu, W.; Huang, Y.; Li, G. Fatigue test of semi-rigid base Materials. *Highway* **1991**, *9*, 31–34.
32. Tian, H.; Zheng, C.; Qin, Y.; Lv, D.; Zhang, T. Research on fatigue cracking control Factors of semi-rigid base asphalt concrete Pavement. *Highway* **2014**, *59*, 32–36.
33. Zhu, J.; Guo, F. Experimental study on anti-aging performance of polymer modified high toughness cement-based composite concrete pavement. *Chem. Bond.* **2024**, *46*, 65–70.
34. GB 175-2007; Common Portland Cement. Standards Press of China: Beijing, China, 2007.
35. JTG E30-2005; Test Methods of Cement and Concrete for Highway Engineering. China Communications Press: Beijing, China, 2005.
36. JTG/T F20-2015; Technical Guidelines for Construction of Highway Roadbases. China Communications Press: Beijing, China, 2015.
37. JTG E42-2005; Test Methods of Aggregate for Highway Engineering. China Communications Press: Beijing, China, 2016.
38. GB/T 33281-2016; Welded Wire Fabric Coated with Zinc. Standards Press of China: Beijing, China, 2016.
39. GB/T 1839-2008; Test Method for Gravimetric Determination of the Mass per Unit Area of Galvanized Coatings on Steel Products. Standards Press of China: Beijing, China, 2008.
40. GB/T 228.1-2021; Metallic Materials—Tensile Testing—Part 1: Method of Test at Room Temperature. Standards Press of China: Beijing, China, 2021.
41. GB/T 17689-2008; Geosynthetics—Plastic Geogrids. Standards Press of China: Beijing, China, 2008.
42. GB/T 21825-2008; Glass Fibre Geogrid. Standards Press of China: Beijing, China, 2008.
43. Ye, H.; Tang, S.; Duan, Z. Orthotropic composite bridge of steel fiber reinforced concrete panel fatigue test research. *Highway* **2022**, *3*, 115–121. [[CrossRef](#)]
44. Wang, F.; Xie, S. Research on Mulative Fatigue Damage of Asphalt Pavement Based on Multi-level Amplitude Loading. *Highw. Eng.* **2017**, *42*, 267–272.
45. Kim, Y.K.; Park, J.Y.; Han, S.H.; Lee, S.W. Investigation of Fatigue Characteristics of Roller-Compacted Concrete Pavement based on Full-Scale Fatigue Test and Accelerated Pavement Test. In Proceedings of the 1st International Conference for Road Engineers, Jeju, Republic of Korea, 29 May–1 June 2018.
46. Cui, X. Research on the Development Law of Semi-Rigid Base Structure and Material Properties. Master's Thesis, Southeast University, Nanjing, China, 2020.
47. Guo, F. Permanent Pavement Semi-Rigid Base Fatigue Characteristics Analysis and Research. Master's Thesis, Chongqing Jiaotong University, Chongqing, China, 2023.
48. Zou, J.R.; Zhang, Z.Q.; Tao, L.I. Failure Mechanism and Control Measures of Common Trunk Highway Semi-rigid Base Asphalt Pavement. *J. Highw. Transp. Res. Dev.* **2018**, *35*, 1–7.

**Disclaimer/Publisher's Note:** The statements, opinions and data contained in all publications are solely those of the individual author(s) and contributor(s) and not of MDPI and/or the editor(s). MDPI and/or the editor(s) disclaim responsibility for any injury to people or property resulting from any ideas, methods, instructions or products referred to in the content.